ROYAL SOCIETY OF CHEMISTRY

PAPER

Check for updates

Single-crystalline MAPbCl₃ thin-films for photo- and X-ray voltaics

Waqas Zia,[ab] Mahdi Malekshahi Byranvand,*[a] Vishal Yeddu,[c] Yuki Haruta,[c] Dongyang Zhang,[c] Makhsud I. Saidaminov [ID] *[cd] and Michael Saliba [ID] *[ab]

3 eV wide bandgap methylammonium lead trichloride (MAPbCl₃) perovskites are promising for transparent solar cells, smart windows, and the internet of things (IoTs). However, it is challenging to crystallize uniform polycrystalline MAPbCl₃ thin films from solution. On the other hand, single-crystalline MAPbCl₃ can be grown as relatively uniform thin films. In this work, we demonstrate the fabrication of single-crystalline MAPbCl₃ thin films on conductive glass substrates *via* a space-confined inverse temperature crystallization (ITC). The perovskite films exhibit no emission peaks from states located deep within the bandgap, confirming a less defective perovskite bulk than its polycrystalline counterpart. The resulting perovskite solar cells (PSCs) yield an open-circuit voltage (V_{OC}) of up to 1.64 V and a high power conversion efficiency (PCE) of 1.1% under one sun irradiation. Additionally, the MAPbCl₃ is studied for its conversion of X-rays into electrical energy, *i.e.*, "X-ray-voltaics", demonstrating a V_{OC} of 0.89 V together with an output power of 3.57 μW cm⁻² at an X-ray tube voltage of 60 kV (4900 μW cm⁻²).

Broader context

While narrow-bandgap perovskites have been central to the development of high-efficiency solar cells, wide-bandgap counterparts, like MAPbCl₃, are gaining interest. Its inherent transparency and the ability to yield high open-circuit voltages make it well-suited for applications like smart windows and advanced sensor systems, which can operate at very low current inputs. However, achieving a uniform polycrystalline MAPbCl₃ defect-free thin film remains a significant challenge. We have demonstrated that growing single-crystalline thin films of MAPbCl₃ *via* inverse temperature crystallization results in highly crystalline thin films with minimal deep trap states, without requiring post-treatment. Apart from employing these single-crystalline MAPbCl₃ thin films for the first time as solar cells, we also extend their use to X-ray voltaic devices. Notably, under X-ray exposure, wide-bandgap perovskites outperform their narrow-bandgap perovskites, an inverse trend compared to performance under solar illumination. This broadens the scope of MAPbCl₃ beyond traditional photovoltaics, like industrial inspection, space radiation monitoring, and medical diagnostics. These diverse functionalities broaden the prospects of possible commercialization pathways of perovskites.

Introduction

Metal-halide perovskite solar cells (PSCs) have attracted much attention in recent years due to their excellent optoelectronic properties[1–4] based primarily on polycrystalline perovskite thin films. Despite their excellent progress in power conversion efficiencies (PCEs), the open-circuit voltage (V_{OC}) deficit (compared to the bandgap) for wide bandgap perovskites can still be improved.[5–7]

Recently, we have reported, to our knowledge, the hitherto highest V_{OC} of 1.78 V for single-junction PSCs based on

methylammonium lead chloride (MAPbCl₃).[8] However, considering the wide bandgap (E_g) of 3.03 eV for MAPbCl₃, there is still a significant loss-in-potential (*i.e.*, $E_g/q - V_{OC}$), since the potential V_{OC} for MAPbCl₃ is 2.69 V (corresponding to a loss-in-potential of 0.34 V).[9] Our work has shown that the crystallization of MAPbCl₃ thin films with a homogenous morphology and a uniform interface is quite challenging because of the lower solubility of chloride salts in organic solvents and fast crystallization kinetics. This results in excessive non-radiative recombination, leading to a considerable loss-in-potential.[8]

However, the solution-grown cubic and transparent bulk MAPbCl₃ single crystals have been used for photodetector applications.[10,11] On a similar basis, PSCs based on single-crystalline films have been demonstrated using various perovskites, *e.g.*, MAPbI₃ (1.55 eV), MAPbBr₃ (2.3 eV), FA₀.₆MA₀.₄PbI₃ (1.48 eV), and FAPbI₃ (1.5 eV).[12–15] However, in contrast to bulk perovskite single crystals, which are many centimeters in size, growing single-crystalline films on the substrate is challenging because of unwanted nucleation sites, control of thickness, and

[a]Institute for Photovoltaics (ipv), University of Stuttgart, 70569 Stuttgart, Germany. E-mail: mahdi.malekshahi@ipv.uni-stuttgart.de; michael.saliba@ipv.uni-stuttgart.de

[b]Helmholtz Young Investigator Group FRONTRUNNER, IMD-3 Photovoltaics, Forschungszentrum Jülich, Jülich, 52425, Germany

[c]Department of Chemistry, University of Victoria, 3800 Finnerty Road, Victoria, British Columbia V8P 5C2, Canada. E-mail: msaidaminov@uvic.ca

[d]Department of Electrical & Computer Engineering, University of Victoria, 3800 Finnerty Road, Victoria, British Columbia V8P 5C2, Canada

growth dynamics. One method for answering these challenges is the space-confined inverse temperature crystallization (ITC) method that has been used for single-crystalline thin films.[16,17]

Additionaly, these single-crystalline thin films, due to their relatively high thicknesses, can also absorb more effectively high-energy neutrons, alpha (α) particles, beta (β) particles, and X-rays into electrical energy.[18,19] Zhao and co-workers have demonstrated β-voltics based on polycrystalline MAPbBr$_3$ and mixed-cation PSCs. These β-voltaic cells find their applications in space electronics and implantable medical devices due to their long lifespan, high energy density, and durability.[20,21] In contrast, X-rays offer better energy conversion owing to their higher penetration depth than β-particles. For example, MAPbI$_3$ single-crystalline solar cells have recently been tested as X-ray voltaic devices.[22]

A sufficiently thick perovskite film with a wide bandgap is needed to absorb high-energy particles, enhance their energy deposition, and minimize thermal losses. Polycrystalline perovskite thin films are typically limited to ~1 μm. On the other hand, single-crystalline perovskite films are free of grain boundaries, have high charge mobilities, and are relatively thick.[23–26] Here we focus on single-crystalline MAPbCl$_3$ with a wide bandgap that reduces the thermal losses from high-energy particles. In addition, single-crystalline MAPbCl$_3$ films can be crystallized without annealing or post-treatment steps to improve the film morphology. These single-crystalline MAPbCl$_3$ films can be integrated into X-ray voltaic cells to absorb high-energy X-rays, suitable for applications like security screening, flaw detection, and environmental monitoring.[27]

Here, among the first time, we fabricate single-crystalline MAPbCl$_3$ thin films *via* the space-confined ITC method for both photovoltaic and X-ray voltaic applications. The devices, without any passivation or post-treatment steps, show V_{OC}'s of up to 1.64 V with one of the highest PCEs of 1.1%, under one sun illumination. Despite high crystalline quality and absence of grain boundaries, a higher V_{OC} compared to passivated polycrystalline thin films (a few hundred nm's thick) has not been achieved. This can be related to the higher thickness of single-crystalline films (a few μm's thick), which may result in a higher saturation current density due to an increased non-radiative recombination processes. In addition, the diffusion length may not scale according to the layer thickness further inhibiting the V_{OC}. Solar cells using this material are further employed as X-ray voltaic cells. At an X-ray tube voltage of 60 kV (equal to an input power density of 4900 μW cm^{-2}), a V_{OC} of 0.89 V is obtained along with an output power density of 3.57 μW cm^{-2}. According to the best of our knowledge, this is the highest power conversion achieved by X-rays for PSCs. These initial results show that by carefully optimizing the
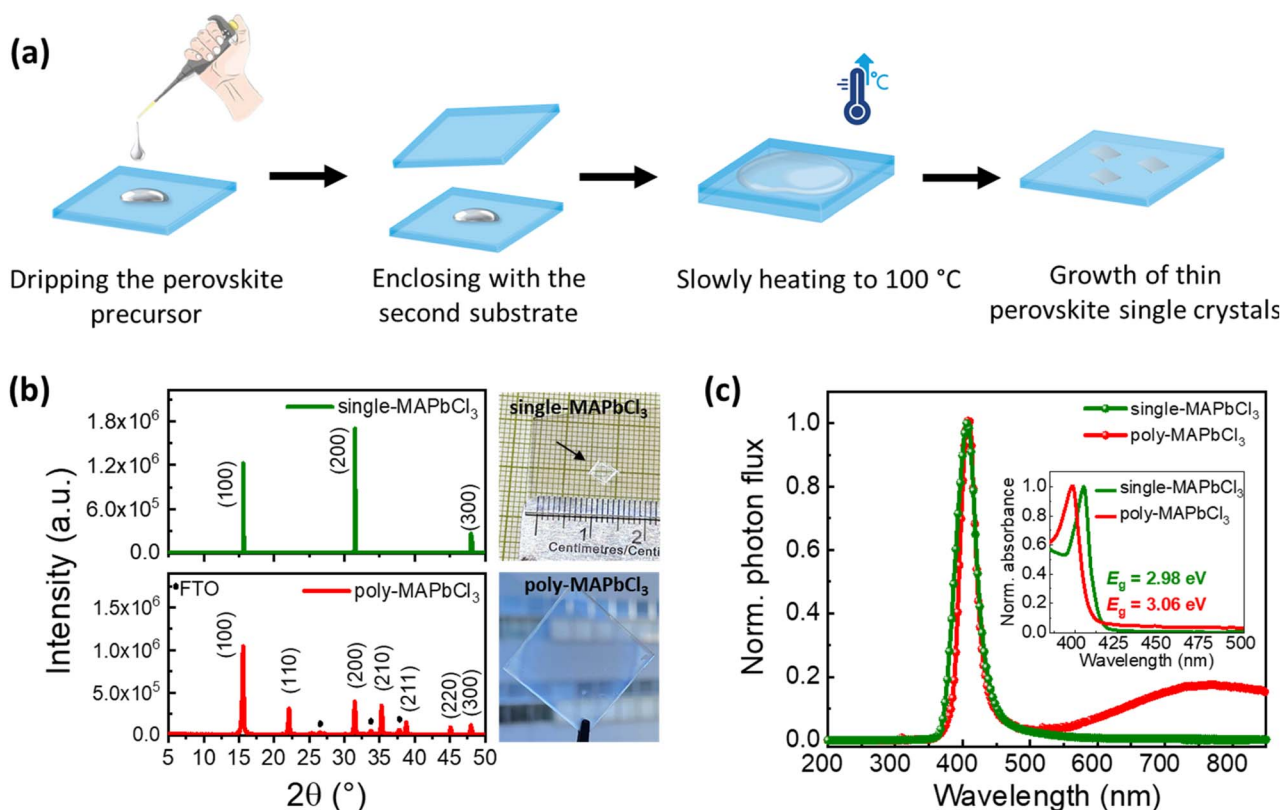

Fig. 1 (a) Schematics showing the steps in fabricating single-crystalline MAPbCl$_3$ solar cells *via* space-confined ITC. (b) XRD spectra of the single-crystalline and polycrystalline MAPbCl$_3$ thin films. (c) Normalized PL spectrum of the single-crystalline and polycrystalline thin films measured at an excitation wavelength of 343 nm (inset: normalized absorbance spectra showing a bandgap of 2.98 eV and 3.06 eV for the single-crystalline and polycrystalline MAPbCl$_3$ thin films respectively (extracted Tauc plots in Fig. S1 in the SI).

crystallization process and thickness of MAPbCl$_3$, an alternative use case can be established for widest bandgap materials.

Results and discussion

Single-crystalline MAPbCl$_3$ thin films are grown by the space-confined ITC method.[16,17] The experimental details can be found in the SI. Briefly, the perovskite precursor solution is sandwiched between two substrates, and the temperature is increased slowly to 100 °C (Fig. 1a). When the solution reaches the supersaturation limit, a single-crystalline thin film grows within the confined space.

We note that single-crystalline MAPbCl$_3$ films form without any additional annealing or passivation step at ambient conditions in air and are highly crystalline. This is confirmed by the crystallographic properties of the obtained MAPbCl$_3$ films *via* X-ray diffraction (XRD), showing intense reflections at (100), (200), and (300) planes at diffraction angles of 15.59°, 31.50°, and 47.98°, respectively. There is no additional diffraction response from other planes (Fig. 1b). When compared to our previously reported polycrystalline MAPbCl$_3$ thin films,[15] additional multiple reflections from different planes can be observed at 22.12°, 35.32°, and 38.78°.

For the optical properties, photoluminescence (PL) measurements for both single- and polycrystalline thin films are performed. Fig. 1c shows the band-to-band radiative recombination peaks at 406 nm in both cases. For the polycrystalline thin film, an additional peak can be observed at 750 nm, indicating a band-to-defect recombination peak. Consistent with our previous findings, this peak confirms the existence of deep defect states in the polycrystalline MAPbCl$_3$ perovskite.[8]

On the other hand, this additional peak has not been observed for the single-crystalline sample, which is consistent with the reduction of deep traps in the bulk. However, the asymmetry of the PL spectrum for single-crystalline MAPbCl$_3$ has already been reported in the literature and is attributed to the presence of Cl$^-$ vacancies at the crystal surface.[11] This highlights that MAPbCl$_3$ appears to be intrinsically more prone to surface defects due to the lower formation energy (-0.7 eV) in chlorine compared to iodine (-0.1 eV) and bromine (0.25 eV)-based perovskites.[28]

The UV-vis absorption spectra of single- and polycrystalline thin films are illustrated in Fig. 1c (inset). The extracted Tauc plot of single-crystalline thin film shows a slightly lower bandgap of 2.98 eV compared to polycrystalline thin film of 3.06 eV (see Fig. S1 in the SI), which follows the reported bandgap values for single-[29] and polycrystalline[30] MAPbCl$_3$ thin films.
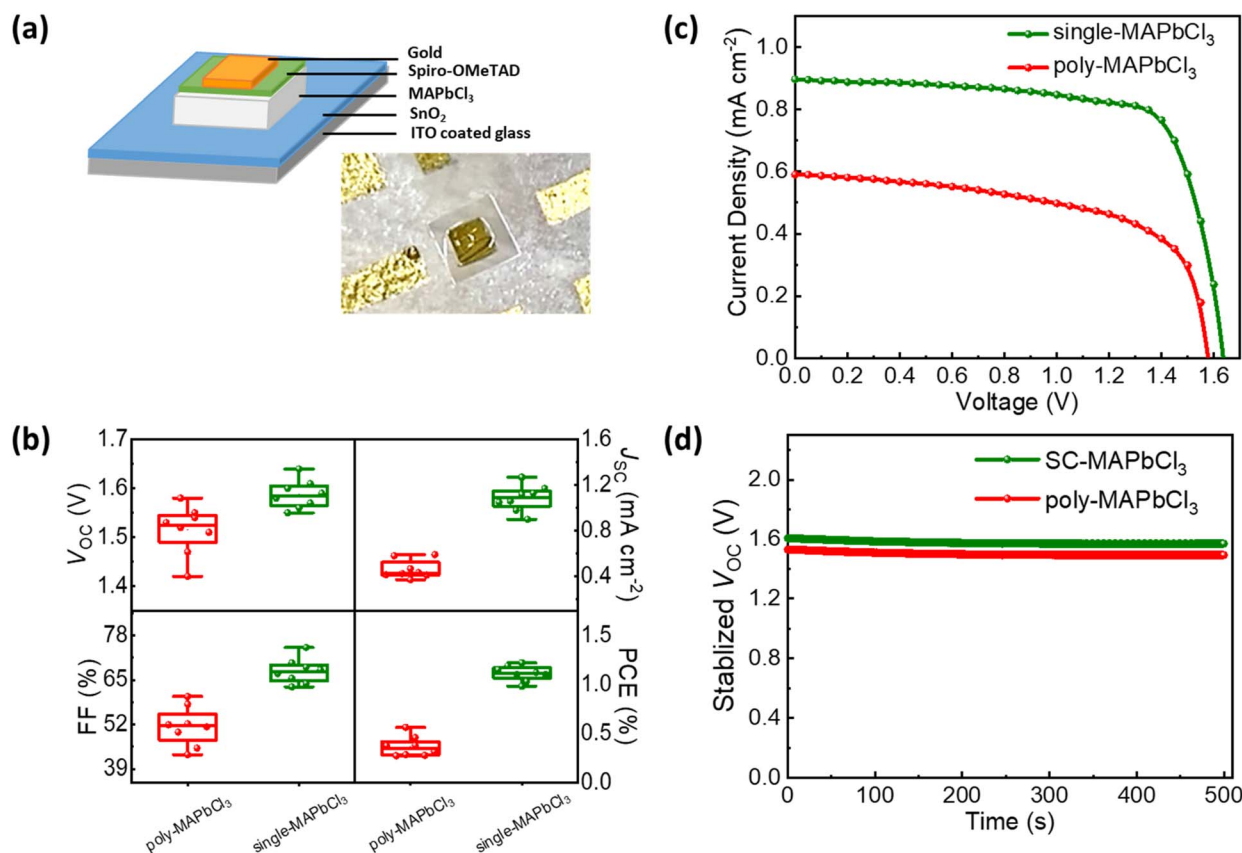

Fig. 2 (a) Layer stack of a single-crystalline MAPbCl$_3$ solar cell with a n-i-p configuration, together with a photograph of a single-crystalline MAPbCl$_3$ solar cell (based on a single crystal of size 2.3 mm × 2.3 mm). (b) Device statistics for V_{OC}, J_{SC}, FF, and PCE of single-crystalline and polycrystalline MAPbCl$_3$ solar cells ($n = 8$ devices). (c) JV-curves of the champion solar cells. (d) Stabilized V_{OC} for 500 s for both single- and polycrystalline MAPbCl$_3$ solar cells.

The narrowing of the bandgap for perovskite single crystals due to their thickness-dependent below-bandgap absorption is well reported in the literature and attributed to the slight transition of direct bandgap to indirect bandgap.[31–33] It has been argued that, for thicker perovskite films, this transition occurs due to the distortion of the lead iodide framework. This results in an electric field across the Pb atom and, hence, splits the conduction band *via* Rashba splitting.[34]

In the next step, we incorporate the single-crystalline films into a solar cell stack of glass/ITO/SnO$_2$/MAPbCl$_3$/Spiro-OMeTAD/Au. Fig. 2a shows a photograph of a single-crystalline MAPbCl$_3$ solar cell (see the Experimental section in SI). On the other hand, polycrystalline MAPbCl$_3$ solar cells are fabricated using a layer stack glass/FTO/c-TiO$_2$/mp-TiO$_2$/MAPbCl$_3$/Spiro-OMeTAD/Au as described in our previous work.[8] We note that due to the poor film coverage of polycrystalline MAPbCl$_3$ films, planar SnO$_2$ electron transport layer (ETL) frequently leads to shunting paths, resulting in non-functional devices, as shown in Fig. S2. Owing to this, a mesoporous TiO$_2$-based ETL is used to avoid shunting, as its mesoporous structure embeds the perovskite efficiently. However, the same mesoporous TiO$_2$ layer might not provide a smooth surface for the growth of single-crystalline thin films, as the underlying mesoporous film would induce unwanted heterogeneous nucleation sites, hampering the formation of single crystals.[35] Hence, a facile, planar SnO$_2$ ETL on an ITO substrate is needed to achieve high-quality single-crystalline MAPbCl$_3$ films.

Fig. 2b shows the statistical data of the photovoltaic parameters for both single- and polycrystalline solar cells with 8 devices in each case under one sun. The single-crystalline devices show remarkable reproducibility with an average V_{OC} = 1.59 ± 0.03 V, short-circuit current density (J_{SC}) = 1.09 ± 0.11

mA cm^{-2}, a fill factor (FF) = 67.6 ± 3.66% and a PCE = 1.11 ± 0.08%. On the other hand, polycrystalline devices show an average V_{OC} of 1.52 ± 0.05 V, J_{SC} = 0.46 ± 0.08 mA cm^{-2}, FF = 51.5 ± 5.73%, and PCE = 0.36 ± 0.10%.

The champion single-crystalline MAbCl$_3$ solar cell results in a V_{OC} of 1.64 V, J_{SC} of 0.9 mA cm^{-2} and a FF of 74.5% with a PCE of 1.10%. To the best of our knowledge, this represents the highest reported PCE for MAPbCl$_3$ solar cells. On the other hand, the champion polycrystalline MAPbCl$_3$ solar cell has yielded a lower V_{OC} of 1.58 V, J_{SC} of 0.59 mA cm^{-2}, and a FF of 60.2%, leading to a significantly lower PCE of 0.56% (see Fig. 2c, Table 1). Since V_{OC} is the main performance criteria for these wide bandgap perovskites with significantly lower currents, we perform long-term V_{OC} tracking on these devices. Fig. 2d shows stabilized V_{OC} for 500 s under constant illumination for both single- and polycrystalline MAPbCl$_3$ thin films, highlighting their significant long-term stability.

Although the single-crystalline MAPbCl$_3$ thin films grown by the space-confined ITC method are of high quality in terms of their crystallinity and optical properties, still, a V_{OC} of 1.64 V is lower than the theoretical limit of 2.69 V for a E_g of ~3.1 eV, as reported by Lunt *et al.*[9]

In our previous work on polycrystalline MAPbCl$_3$ thin films, annealing of the films in MACl vapor atmosphere has resulted into an improved film morphology, leading to a V_{OC} of 1.78 V.[8] Using such post-treatments in various annealing atmospheres here for a prolonged annealing at high temperatures result in the detachment of the single crystals, leading to no electrical contact between MAPbCl$_3$ and the SnO$_2$ ETL. In addition, one of the main reasons for the lower V_{OC} is the higher thickness of single-crystalline thin films, as polycrystalline perovskite thin films grown by spin-coating are typically a few hundred nanometers thick, whereas single-crystalline thin films are usually a few μm's thick. Due to the diffusion length not necessarily scaling with thickness, even an improved bulk quality may preclude charges from diffusing all the way to their (now far away) respective contacts. Fig. 3(a) and (b) show the cross-section scanning electron microscopy (SEM) images of two different single-crystalline MAPbCl$_3$ thin film solar cells consisting of ITO/SnO$_2$/MAPbCl$_3$/spiro-OMeTAD/Au layer stack.

Table 1 Photovoltaic parameters of single- and polycrystalline MAPbCl$_3$ solar cells

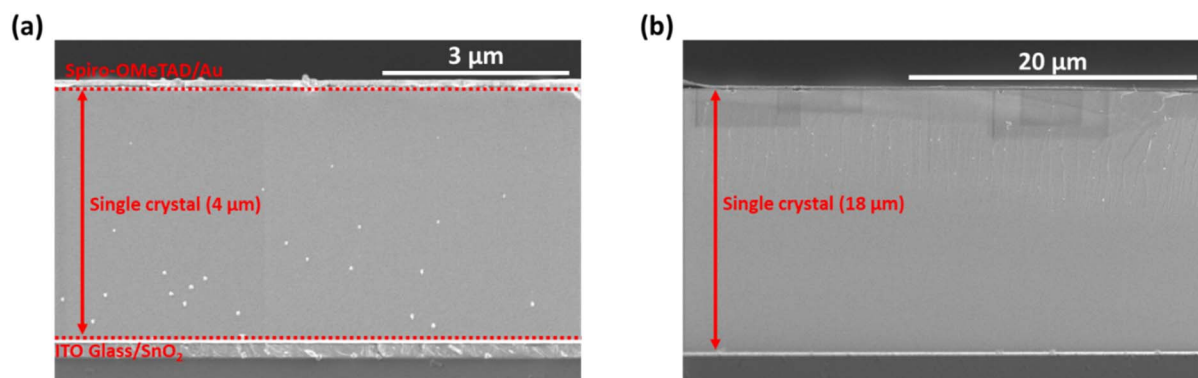|	V_{OC} (V)	J_{SC} (mA cm^{-2})	FF (%)	PCE (%)
poly-MAPbCl$_3$	1.58	0.59	60.2	0.56
single-MAPbCl$_3$	1.64	0.90	74.5	1.10

Fig. 3 SEM cross-section of a single-crystalline MAPbCl$_3$ thin film solar cell (a) with a thickness of ~4 μm (b) with a thickness of ~18 μm.

These images show that the thickness of single-crystalline MAPbCl$_3$ thin films ranges from 4 μm to 18 μm. The diffusion of charge carriers toward the surface of a semiconductor becomes less efficient if the surface lies further away.[36]

This can be further explained with the help of the diode equation for a single junction solar cell $\left(V_{OC} = \frac{nkT}{q} \ln\left(\frac{J_{SC}}{J_0} + 1\right)\right)$, where n is the ideality factor, k is Boltzmann constant, T is the temperature, and J_{SC}, J_0 are the photogenerated and saturation current densities, respectively. The increase in the saturation current density J_0 is generally correlated with the increase in non-radiative recombination in a solar cell and, hence, a decrease in the V_{OC}.[37,38] Kirchartz and co-workers have reported that J_0 within the bulk increases linearly with the increase in the absorber layer thickness. With a thicker perovskite layer, more photons can be absorbed, and hence, more photogenerated charge carriers are produced. However, at the same time, it triggers more non-radiative recombination mechanisms within the perovskite bulk, which leads to significant V_{OC} losses.[39,40] Huang and his team have shown a decrease in the V_{OC} of single-crystalline MAPbI$_3$ solar cells with an increase in the thickness of single-crystalline thin films up to 40 μm.[31] Similarly, Turedi et al. demonstrated that increasing the thickness of the perovskite layer in single-crystalline solar cells led to a decline in device performance, attributed to inefficient charge carrier collection.[41]

One more aspect of this lower V_{OC} is the narrowed bandgap of the perovskite single crystals from 3.03 eV to 2.98 eV. In addition, the fabrication process of thin film single-crystalline solar cells at a μm scale is not yet completely optimized and has its own challenges, such as varying space between the two sandwiched substrates. This leads to a difference in thickness between various single crystals grown on a single substrate. Optimization could entail constant space between the substrates and increasing the amount of precursor between substrates to ensure larger crystals.[42] Furthermore, the thickness of as-grown single-crystalline thin films can be reduced by laser polishing as shown by Kedia et al.[43] This would result in thin single-crystalline layers of uniform thickness with a much smoother interface with the HTL. On the other hand, an increased volume of precursor solution with a lower concentration can help to avoid fast supersaturation and, hence, inhibit the multiple nucleation sites. In addition to that, careful post-treatments need to be defined that may help to improve the surface morphology of these single-crystalline thin films without detaching them from the substrates.

Finally, these devices, as a proof of concept, are further used as X-ray voltaic cells at different X-ray tube voltages. The performance of X-ray voltaic cells is governed by the maximum amount of energy deposited in the perovskite layer. Different factors influence the energy dosage of X-rays in the perovskite layer. The accelerating voltage of the incoming electrons in the X-ray tube and the thickness of the layers lying above the perovskite are very critical. If the accelerating voltage is too low, then most of the energy will be deposited into the front layers before the X-rays reach the perovskite layer. Similarly, if the accelerating voltage is too high, the X-rays will simply penetrate through the perovskite layer, and the according energy would be wasted. Keeping that in mind, in this work, the single-crystalline MAPbCl$_3$ devices have been exposed to X-rays from the Au contact side instead of from the glass side to avoid the energy deposition of X-rays in the thick glass substrate rather than in the perovskite layer.[20]

Since the energy of X-rays is significantly higher than the bandgap of the perovskites, MAPbCl$_3$, with its wide bandgap, can be used for X-ray voltaics. The higher energy of the X-rays results in the formation of hot carriers with high kinetic energy, which equilibrate themselves by dissipating the heat energy to the lattice instead of taking part in the power generation. Hence, I$^-$ and Br$^-$-based narrow bandgap perovskites are (relatively) less efficient for this purpose.[21] Here, MAPbCl$_3$ single-crystalline devices are measured as X-ray voltaic cells using a tungsten-based X-ray tube. Polycrystalline-MAPbCl$_3$ thin films cannot be employed for X-ray voltaics as their thickness is too low for X-rays to deposit any energy, resulting in no current signal. The X-ray beam is collimated using a 10 mm diameter aluminum slit and is directed on the X-ray voltaic cell. The complete schematic of the setup is shown in Fig. 4a. An X-ray image of the X-ray voltaic cell is taken to make sure that the device lies within the focus of the X-ray beam, as shown in Fig. 4b. The X-ray tube voltage is increased from 20 kV to 60 kV at a constant tube current of 1 mA to observe the influence of the tube voltage on the device performance. The corresponding power densities at each tube voltage (calculated via SpekPy[44] and counter checked by Monte Carlo Simulations[45]) range from 500 μW cm^{-2} to 4900 μW cm^{-2}. Currently, our setup is restricted from going beyond 60 kV as it can cause adverse effects on the X-ray tube life.

With increasing the tube voltage, the single-crystalline devices have shown improved X-ray voltaic parameters, as shown in Fig. 4c: at a tube voltage of 20 kV equal to an input power density of 500 μW cm^{-2}, a J_{SC} of 5.40 μA cm^{-2}, along with a V_{OC} of 0.8 V, leading to an output power density of 2.26 μW cm^{-2}. For 40 kV (2300 μW cm^{-2}), J_{SC} and V_{OC} have increased to a value of 6.08 μA cm^{-2} and 0.86 V, respectively, with a power conversion of 3.2 μW cm^{-2}. The highest V_{OC} of 0.89 V with a J_{SC} of 6.73 μA cm^{-2} is obtained at a tube voltage of 60 kV (4900 μW cm^{-2}) with an output power density of 3.57 μW cm^{-2}. The output power curves corresponding to different X-ray input powers have been shown in Fig. 4d. To the best of our knowledge, this is the highest output power achieved by perovskite X-ray voltaic cells. Previously, Moazzezi et al. have reported an output power of 0.33 μW cm^{-2} for single-crystalline MAPbI$_3$-based X-ray voltaic cells.[22] In a similar approach, an output power of ~0.14 μW has been reported for AlGaInP based X-ray voltaics.[46] Our findings further strengthen that wide bandgap perovskites exhibit significantly superior performance compared to narrow bandgap ones, when exposed to radiant sources like X-rays.[21] This is contrary to their trend under one sun condition, where photovoltaic power conversion decreases with the increase in bandgap. This efficient harvesting of radiant energy shows the potential of MAPbCl$_3$ to meet the needs of low-power devices such as micro-electro-mechanical systems (MEMS) during space missions. These self-powered X-
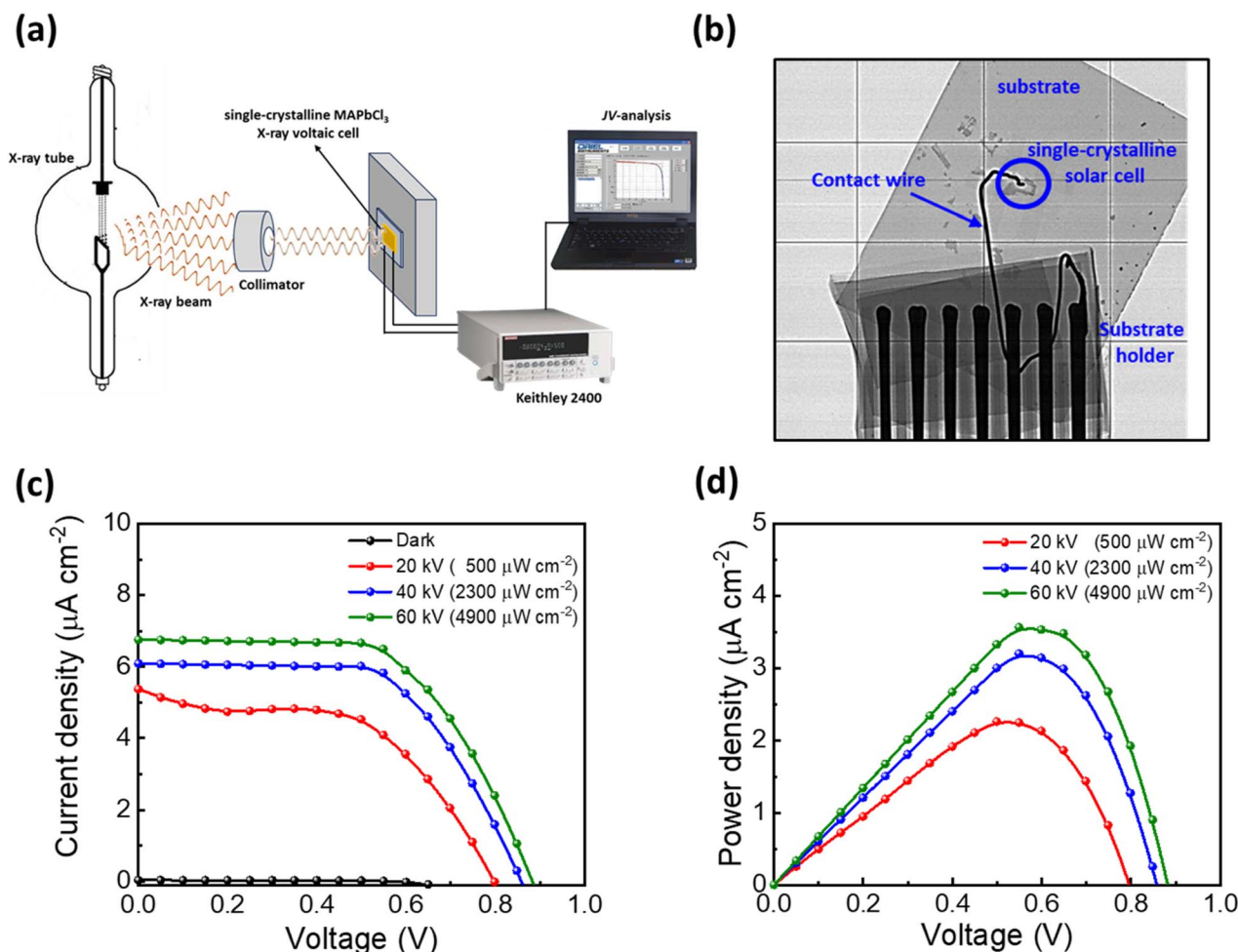
Fig. 4 (a) Schematics of the X-ray voltaic setup consisting of a tungsten-based X-ray tube (b) X-ray image of a single-crystalline MAPbCl$_3$ solar cell on an ITO substrate contacted with a contact wire to measure IV-traces. (c) JV-curves of the champion single-crystalline MAPbCl$_3$ X-ray voltaic cells at different X-ray tube voltages corresponding to different power densities (d) Output power curves of single-crystalline MAPbCl$_3$ X-ray voltaic cells at different X-ray tube voltages.

ray voltaic devices may also eliminate the need for a battery to power the devices.[46]

Moreover, compared to MAPbI$_3$ and MAPbBr$_3$, MAPbCl$_3$ exhibits superior intrinsic stability due to its more negative enthalpy of formation,[47,48] stronger Pb–Cl bonds that inhibit defect formation and degradation,[49,50] and enhanced resistance to moisture.[51] These characteristics make it particularly well-suited for the environments and applications discussed above. At the same time, there is still significant scope for improving the device's performance under X-ray irradiation. For example, the thickness of perovskite, ETL, HTL, and metallic thin films could be further optimized such that the maximum energy deposition occurs in the absorber layer. Furthermore, standardized measurement conditions for X-ray voltaics are also very crucial for enhancing their performance.

Conclusion

In conclusion, we demonstrate the potential of MAPbCl$_3$ perovskite in the form of single-crystalline thin films for both photo and X-ray voltaics. Our results show that, compared to polycrystalline thin films, high-quality single-crystalline MAPbCl$_3$ thin films can be crystallized out without any annealing or passive step. These single-crystalline thin films result in a V_{OC} of 1.64 V and a PCE of 1.10%. At the same time, currently, the increased thickness of single-crystalline thin films results in enhanced non-radiative recombination processes affecting the overall diffusion of the charge carriers, leading to a relatively lower V_{OC}. As a proof of concept, these single-crystalline MAPbCl$_3$ thin films are further employed as X-ray voltaic cells. At a tube voltage of 60 kV, this leads to a V_{OC} of 0.89 V and a remarkable output power of 3.57 μW cm^{-2}, highlighting the potential of the widest bandgap perovskites for novel use cases beyond solar applications.

Conflicts of interest

There are no conflicts to declare.

Data availability

The data will be available upon reasonable request.

Experimental details, characterization methods, Tauc plots, and *JV*-curve of a planar shunted polycrystalline solar cell are available in the supplementary information. See DOI: https://doi.org/10.1039/d5el00087d.

Acknowledgements

References

1 A. Kojima, K. Teshima, Y. Shirai and T. Miyasaka, Organometal Halide Perovskites as Visible-Light Sensitizers for Photovoltaic Cells, *J. Am. Chem. Soc.*, 2009, **131**(17), 6050–6051, DOI: 10.1021/ja809598r.

2 M. Saliba, T. Matsui, J.-Y. Seo, K. Domanski, J.-P. Correa-Baena, M. Khaja Nazeeruddin, S. M. Zakeeruddin, W. Tress, A. Abate, A. Hagfeldt and M. Grätzel, Cesium-Containing Triple Cation Perovskite Solar Cells: Improved Stability, Reproducibility and High Efficiency, *Energy Environ. Sci.*, 2016, **9**(6), 1989–1997, DOI: 10.1039/C5EE03874J.

3 Y. Rong, Y. Hu, A. Mei, H. Tan, M. I. Saidaminov, S. I. Seok, M. D. McGehee, E. H. Sargent and H. Han, Challenges for Commercializing Perovskite Solar Cells, *Science*, 2018, **361**(6408), eaat8235, DOI: 10.1126/science.aat8235.

4 S. M. Park, M. Wei, J. Xu, H. R. Atapattu, F. T. Eickemeyer, K. Darabi, L. Grater, Y. Yang, C. Liu, S. Teale, B. Chen, H. Chen, T. Wang, L. Zeng, A. Maxwell, Z. Wang, K. R. Rao, Z. Cai, S. M. Zakeeruddin, J. T. Pham, C. M. Risko, A. Amassian, M. G. Kanatzidis, K. R. Graham, M. Grätzel and E. H. Sargent, Engineering Ligand Reactivity Enables High-Temperature Operation of Stable Perovskite Solar Cells, *Science*, 2023, **381**(6654), 209–215, DOI: 10.1126/science.adi4107.

5 N. Marinova, S. Valero and J. L. Delgado, Organic and Perovskite Solar Cells: Working Principles, Materials and Interfaces, *J. Colloid Interface Sci.*, 2017, **488**, 373–389, DOI: 10.1016/j.jcis.2016.11.021.

6 M. Daboczi, I. Hamilton, S. Xu, J. Luke, S. Limbu, J. Lee, M. A. McLachlan, K. Lee, J. R. Durrant, I. D. Baikie and J.-S. Kim, Origin of Open-Circuit Voltage Losses in Perovskite Solar Cells Investigated by Surface Photovoltage Measurement, *ACS Appl. Mater. Interfaces*, 2019, **11**(50), 46808–46817, DOI: 10.1021/acsami.9b16394.

7 W. Tress, Perovskite Solar Cells on the Way to Their Radiative Efficiency Limit – Insights Into a Success Story of High Open-Circuit Voltage and Low Recombination, *Adv. Energy Mater.*, 2017, **7**(14), 1602358, DOI: 10.1002/aenm.201602358.

8 W. Zia, M. Malekshahi Byranvand, T. Rudolph, M. Rai, M. Kot, C. Das, M. Kedia, M. Zohdi, W. Zuo, V. Yeddu, M. I. Saidaminov, J. I. Flege, T. Kirchartz and M. Saliba, $MAPbCl_3$ Light Absorber for Highest Voltage Perovskite Solar Cells, *ACS Energy Lett.*, 2024, **9**(3), 1017–1024, DOI: 10.1021/acsenergylett.3c02777.

9 D. Liu, C. Yang and R. R. Lunt, Halide Perovskites for Selective Ultraviolet-Harvesting Transparent Photovoltaics, *Joule*, 2018, **2**(9), 1827–1837, DOI: 10.1016/j.joule.2018.06.004.

10 Z. Chen, C. Li, A. A. Zhumekenov, X. Zheng, C. Yang, H. Yang, Y. He, B. Turedi, O. F. Mohammed, L. Shen and O. M. Bakr, Solution-Processed Visible-Blind Ultraviolet Photodetectors with Nanosecond Response Time and High Detectivity, *Adv. Opt. Mater.*, 2019, **7**(19), 1900506, DOI: 10.1002/adom.201900506.

11 H.-P. Hsu, L.-C. Li, M. Shellaiah and K. W. Sun, Structural, Photophysical, and Electronic Properties of $CH_3NH_3PbCl_3$ Single Crystals, *Sci. Rep.*, 2019, **9**(1), 13311, DOI: 10.1038/s41598-019-49926-z.

12 Y. Alsalloum A., B. Turedi, K. Almasabi, X. Zheng, R. Naphade, S. D. Stranks, F. Mohammed O. and M. Bakr O., 22.8%-Efficient Single-Crystal Mixed-Cation Inverted Perovskite Solar Cells with a near-Optimal Bandgap, *Energy Environ. Sci.*, 2021, **14**(4), 2263–2268, DOI: 10.1039/D0EE03839C.

13 W. Peng, L. Wang, B. Murali, K.-T. Ho, A. Bera, N. Cho, C.-F. Kang, V. M. Burlakov, J. Pan, L. Sinatra, C. Ma, W. Xu, D. Shi, E. Alarousu, A. Goriely, J.-H. He, O. F. Mohammed, T. Wu and O. M. Bakr, Solution-Grown Monocrystalline Hybrid Perovskite Films for Hole-Transporter-Free Solar Cells, *Adv. Mater.*, 2016, **28**(17), 3383–3390, DOI: 10.1002/adma.201506292.

14 H.-S. Rao, B.-X. Chen, X.-D. Wang, D.-B. Kuang and C.-Y. Su, A Micron-Scale Laminar MAPbBr₃ Single Crystal for an Efficient and Stable Perovskite Solar Cell, *Chem. Commun.*, 2017, **53**(37), 5163–5166, DOI: **10.1039/C7CC02447A**.

15 P. Moazzezi, V. Yeddu, I. T. Cheong, M. R. Kokaba, S. Dayneko, Y. Ahmed and M. I. Saidaminov, Discovery of Perovskite Cosolvency and Undoped FAPbI₃ Single-Crystal Solar Cells Fabricated in Ambient Air, *J. Am. Chem. Soc.*, 2025, **147**(12), 10203–10211, DOI: **10.1021/jacs.4c15716**.

16 Z. Chen, B. Turedi, A. Y. Alsalloum, C. Yang, X. Zheng, I. Gereige, A. AlSaggaf, O. F. Mohammed and O. M. Bakr, Single-Crystal MAPbI₃ Perovskite Solar Cells Exceeding 21% Power Conversion Efficiency, *ACS Energy Lett.*, 2019, **4**(6), 1258–1259, DOI: **10.1021/acsenergylett.9b00847**.

17 A. Y. Alsalloum, B. Turedi, X. Zheng, S. Mitra, A. A. Zhumekenov, K. J. Lee, P. Maity, I. Gereige, A. AlSaggaf, I. S. Roqan, O. F. Mohammed and O. M. Bakr, Low-Temperature Crystallization Enables 21.9% Efficient Single-Crystal MAPbI₃ Inverted Perovskite Solar Cells, *ACS Energy Lett.*, 2020, **5**(2), 657–662, DOI: **10.1021/acsenergylett.9b02787**.

18 K. Sakhatskyi, B. Turedi, G. J. Matt, E. Wu, A. Sakhatska, V. Bartosh, M. N. Lintangpradipto, R. Naphade, I. Shorubalko, O. F. Mohammed, S. Yakunin, O. M. Bakr and M. V. Kovalenko, Stable Perovskite Single-Crystal X-Ray Imaging Detectors with Single-Photon Sensitivity, *Nat. Photon.*, 2023, **17**(6), 510–517, DOI: **10.1038/s41566-023-01207-y**.

19 Y. He, Z. Liu, K. M. McCall, W. Lin, D. Y. Chung, B. W. Wessels and M. G. Kanatzidis, Perovskite CsPbBr₃ Single Crystal Detector for Alpha-Particle Spectroscopy, *Nucl. Instrum. Methods Phys. Res., Sect. A*, 2019, **922**, 217–221, DOI: **10.1016/j.nima.2019.01.008**.

20 Z. Song, C. Zhao, F. Liao and Y. Zhao, Perovskite-Betavoltaic Cells: A Novel Application of Organic–Inorganic Hybrid Halide Perovskites, *ACS Appl. Mater. Interfaces*, 2019, **11**(36), 32969–32977, DOI: **10.1021/acsami.9b09952**.

21 G. Li, C. Zhao, Y. Liu, J. Ren, Z. Zhang, H. Di, W. Jiang, J. Mei and Y. Zhao, High-Performance Perovskite Betavoltaics Employing High-Crystallinity MAPbBr₃ Films, *ACS Omega*, 2021, **6**(30), 20015–20025, DOI: **10.1021/acsomega.1c03053**.

22 P. Moazzezi, V. Yeddu, S. Dayneko, Y. Haruta, M. R. Kokaba, D. Richtsmeier, Y. Ahmed, A. Amaro, M. Bazalova-Carter, A. M. Navarrete-López and M. I. Saidaminov, Kinetics of Space-Confined Inverse Temperature Crystallization: Gradients Enlarge Thin Perovskite Single Crystals, *ACS Mater. Lett.*, 2024, **6**(8), 3557–3563, DOI: **10.1021/acsmaterialslett.4c00740**.

23 X. Cheng, S. Yang, B. Cao, X. Tao and Z. Chen, Single Crystal Perovskite Solar Cells: Development and Perspectives, *Adv. Funct. Mater.*, 2020, **30**(4), 1905021, DOI: **10.1002/adfm.201905021**.

24 M. Ghasemi, S. Yuan, J. Fan, B. Jia and X. Wen, Challenges in the Development of Metal-Halide Perovskite Single Crystal Solar Cells, *J. Mater. Chem. A*, 2023, **11**(8), 3822–3848, DOI: **10.1039/D2TA08827D**.

25 J. Siekmann, S. Ravishankar and T. Kirchartz, Apparent Defect Densities in Halide Perovskite Thin Films and Single Crystals, *ACS Energy Lett.*, 2021, **6**(9), 3244–3251, DOI: **10.1021/acsenergylett.1c01449**.

26 S. Ravishankar, T. Unold and T. Kirchartz, Comment on "Resolving Spatial and Energetic Distributions of Trap States in Metal Halide Perovskite Solar Cells.", *Science*, 2021, **371**(6532), eabd8014, DOI: **10.1126/science.abd8014**.

27 Y. Wu, J. Feng, Z. Yang, Y. Liu and S. Liu, Halide Perovskite: A Promising Candidate for Next-Generation X-Ray Detectors, *Adv. Sci.*, 2023, **10**(1), 2205536, DOI: **10.1002/advs.202205536**.

28 A. Buin, R. Comin, J. Xu, A. H. Ip and E. H. Sargent, Halide-Dependent Electronic Structure of Organolead Perovskite Materials, *Chem. Mater.*, 2015, **27**(12), 4405–4412, DOI: **10.1021/acs.chemmater.5b01909**.

29 G. Maculan, A. D. Sheikh, A. L. Abdelhady, M. I. Saidaminov, M. A. Haque, B. Murali, E. Alarousu, O. F. Mohammed, T. Wu and O. M. Bakr, CH₃NH₃PbCl₃ Single Crystals: Inverse Temperature Crystallization and Visible-Blind UV-Photodetector, *J. Phys. Chem. Lett.*, 2015, **6**(19), 3781–3786, DOI: **10.1021/acs.jpclett.5b01666**.

30 E. Zheng, B. Yuh, G. A. Tosado and Q. Yu, Solution-Processed Visible-Blind UV-A Photodetectors Based on CH₃NH₃PbCl₃ Perovskite Thin Films, *J. Mater. Chem. C*, 2017, **5**(15), 3796–3806, DOI: **10.1039/C7TC00639J**.

31 Z. Chen, Q. Dong, Q. Liu, C. Bao, Y. Fang, Y. Lin, S. Tang, Q. Wang, X. Xiao, Y. Bai, Y. Deng and J. Huang, Thin Single Crystal Perovskite Solar Cells to Harvest Below-Bandgap Light Absorption, *Nat. Commun.*, 2017, **8**(1), 1890, DOI: **10.1038/s41467-017-02039-5**.

32 E. M. Hutter, M. C. Gélvez-Rueda, A. Osherov, V. Bulović, F. C. Grozema, S. D. Stranks and T. J. Savenije, Direct–Indirect Character of the Bandgap in Methylammonium Lead Iodide Perovskite, *Nat. Mater.*, 2017, **16**(1), 115–120, DOI: **10.1038/nmat4765**.

33 C. Motta, F. El-Mellouhi, S. Kais, N. Tabet, F. Alharbi and S. Sanvito, Revealing the Role of Organic Cations in Hybrid Halide Perovskite CH₃NH₃PbI₃, *Nat. Commun.*, 2015, **6**(1), 7026, DOI: **10.1038/ncomms8026**.

34 T. Wang, B. Daiber, J. M. Frost, S. C. A. Mann, E. Garnett, A. Walsh and B. Ehrler, Indirect to Direct Bandgap Transition in Methylammonium Lead Halide Perovskite, *Energy Environ. Sci.*, 2017, **10**(2), 509–515, DOI: **10.1039/C6EE03474H**.

35 G. Chen, X. Liu, J. An, S. Wang, X. Zhao, Z. Gu, C. Yuan, X. Xu, J. Bao, H.-S. Hu, J. Li and X. Wang, Nucleation-Mediated Growth of Chiral 3D Organic–Inorganic Perovskite Single Crystals, *Nat. Chem.*, 2023, **15**(11), 1581–1590, DOI: **10.1038/s41557-023-01290-2**.

36 A. B. Sproul, Dimensionless Solution of the Equation Describing the Effect of Surface Recombination on Carrier Decay in Semiconductors, *J. Appl. Phys.*, 1994, **76**(5), 2851–2854, DOI: **10.1063/1.357521**.

37 P. Singh and N. M. Ravindra, Temperature Dependence of Solar Cell Performance—an Analysis, *Sol. Energy Mater. Sol. Cells*, 2012, **101**, 36–45, DOI: **10.1016/j.solmat.2012.02.019**.

38 A. Marti, J. L. Balenzategui and R. F. Reyna, Photon Recycling and Shockley's Diode Equation, *J. Appl. Phys.*, 1997, **82**(8), 4067, DOI: 10.1063/1.365717.

39 I. Zonno, B. Krogmeier, V. Katte, D. Lübke, A. Martinez-Otero and T. Kirchartz, Discriminating between Surface and Bulk Recombination in Organic Solar Cells by Studying the Thickness Dependence of the Open-Circuit Voltage, *Appl. Phys. Lett.*, 2016, **109**(18), 183301, DOI: 10.1063/1.4966613.

40 D. Lübke, P. Hartnagel, M. Hülsbeck and T. Kirchartz, Understanding the Thickness and Light-Intensity Dependent Performance of Green-Solvent Processed Organic Solar Cells, *ACS Mater. Au*, 2023, **3**(3), 215–230, DOI: 10.1021/acsmaterialsau.2c00070.

41 B. Turedi, M. N. Lintangpradipto, O. J. Sandberg, A. Yazmaciyan, G. J. Matt, A. Y. Alsalloum, K. Almasabi, K. Sakhatskyi, S. Yakunin, X. Zheng, R. Naphade, S. Nematulloev, V. Yeddu, D. Baran, A. Armin, M. I. Saidaminov, M. V. Kovalenko, O. F. Mohammed and O. M. Bakr, Single-Crystal Perovskite Solar Cells Exhibit Close to Half A Millimeter Electron-Diffusion Length, *Adv. Mater.*, 2022, **34**(47), 2202390, DOI: 10.1002/adma.202202390.

42 L. De Marco, G. Nasti, A. Abate and A. Rizzo, Perovskite Single-Crystal Solar Cells: Advances and Challenges, *Sol. RRL*, 2022, **6**(7), 2101085, DOI: 10.1002/solr.202101085.

43 M. Kedia, M. Rai, H. Phirke, C. A. Aranda, C. Das, V. Chirvony, S. Boehringer, M. Kot, M. M. Byranvand, J. I. Flege, A. Redinger and M. Saliba, Light Makes Right: Laser Polishing for Surface Modification of Perovskite Solar Cells, *ACS Energy Lett.*, 2023, **8**(6), 2603–2610, DOI: 10.1021/acsenergylett.3c00469.

44 G. Poludniowski, A. Omar, R. Bujila and P. Andreo, Technical Note: SpekPy v2.0—a Software Toolkit for Modeling X-Ray Tube Spectra, *Med. Phys.*, 2021, **48**(7), 3630–3637, DOI: 10.1002/mp.14945.

45 M. Bazalova-Carter and N. Esplen, On the Capabilities of Conventional X-Ray Tubes to Deliver Ultra-High (FLASH) Dose Rates, *Med. Phys.*, 2019, **46**(12), 5690–5695, DOI: 10.1002/mp.13858.

46 Y. Wu, Z. Xu, Y. Liu, T. Jiang, H. San and X. Tang, Research on X-Ray-Based Energy Conversion Technology and Assessment of Application Prospect, *Sustain. Energy Technol. Assessments*, 2023, **60**, 103552, DOI: 10.1016/j.seta.2023.103552.

47 A. Senocrate, G. Y. Kim, M. Grätzel and J. Maier, Thermochemical Stability of Hybrid Halide Perovskites, *ACS Energy Lett.*, 2019, **4**(12), 2859–2870, DOI: 10.1021/acsenergylett.9b01605.

48 B. Brunetti, C. Cavallo, A. Ciccioli, G. Gigli and A. Latini, On the Thermal and Thermodynamic (In)Stability of Methylammonium Lead Halide Perovskites, *Sci. Rep.*, 2016, **6**(1), 31896, DOI: 10.1038/srep31896.

49 M. Caputo, N. Cefarin, A. Radivo, N. Demitri, L. Gigli, J. R. Plaisier, M. Panighel, G. Di Santo, S. Moretti, A. Giglia, M. Polentarutti, F. De Angelis, E. Mosconi, P. Umari, M. Tormen and A. Goldoni, Electronic Structure of $MAPbI_3$ and $MAPbCl_3$: Importance of Band Alignment, *Sci. Rep.*, 2019, **9**, 15159, DOI: 10.1038/s41598-019-50108-0.

50 L. McGovern, M. H. Futscher, L. A. Muscarella and B. Ehrler, Understanding the Stability of $MAPbBr_3$ *versus* $MAPbI_3$: Suppression of Methylammonium Migration and Reduction of Halide Migration, *J. Phys. Chem. Lett.*, 2020, **11**(17), 7127–7132, DOI: 10.1021/acs.jpclett.0c01822.

51 U.-G. Jong, C.-J. Yu, G.-C. Ri, A. P. McMahon, N. M. Harrison, P. R. F. Barnes and A. Walsh, Influence of Water Intercalation and Hydration on Chemical Decomposition and Ion Transport in Methylammonium Lead Halide Perovskites, *J. Mater. Chem. A*, 2018, **6**(3), 1067–1074, DOI: 10.1039/C7TA09112E.

© 2025 The Author(s). Published by the Royal Society of Chemistry